

# Source time function clustering reveals patterns in earthquake dynamics

Jiuxun Yin<sup>1</sup>, Zefeng Li<sup>2</sup>, Marine Denolle<sup>1</sup>

<sup>1</sup>Department of Earth and Planetary Sciences, Harvard University, Cambridge, MA, USA

<sup>2</sup>Seismological Laboratory, Division of Geological and Planetary Sciences, California Institute of Technology, Pasadena, CA, USA

## Key Points:

- We cluster earthquakes based on the dynamic time warping distance of their source time function (STF) shapes.
- The patterns of complexity correlate with source parameters such as depth, mechanism, and radiation.
- Simulations of dynamic rupture indicate a correlation between the STF complexity and frictional properties.

---

Corresponding author: Zefeng Li, [zefengli@caltech.edu](mailto:zefengli@caltech.edu)

**Abstract**

We cluster a global data base of 3529  $M > 5.5$  earthquakes in 1995-2018 based on a dynamic time warping dissimilarity of their source time functions (STFs). The clustering exhibits different degrees of STF shape complexity and suggests an association between STF complexity and earthquake source parameters. Thrust events are in large proportion with simple STF shapes and at all depths. In contrast, earthquakes with complex STF shapes tend to be located at shallow depth in complicated tectonic regions with preferentially strike slip mechanism and relatively longer duration. With 2D dynamic modeling of earthquake ruptures on heterogeneous pre-stress and linear slip-weakening friction, we find a systematic variation of the simulated STF complexity with frictional properties. Comparison between the observed and synthetic clustering distributions provides useful constraints on elements of the frictional properties. In particular, the characteristic slip-weakening distance could be constrained to be generally short ( $< 0.1$  m) and depth dependent.

**Plain Language Summary**

Seismic waves carry a signature about the earthquake source process. Earthquake source time functions (STFs), which are directly recovered from seismic waves, reflect the temporal history of earthquake rupture. However, it is often hard to directly compare STFs due to the large differences among earthquakes in terms of amplitude and duration. In this study, we perform a cluster analysis of STFs using a technique called dynamic time warping (DTW). DTW is commonly used in speech recognition to handle with various speeds of elocution. DTW allows us to dynamically stretch the seismic signals and provides a new way to quantify earthquake similarity through analyzing the shapes of their source time functions (STFs). We apply this to a large database of STFs. Our results show that the shape complexity of STFs is correlated with the earthquake source parameters such as the earthquake depth, focal mechanism, and energy radiation. Our numerical simulations further show that those correlations may indicate a spatial heterogeneity of frictional properties.

**1 Introduction**

Earthquakes are known to break in diverse manners: some events rupture on a geometrically simple fault with a relatively smooth slip distribution (e.g., Yagi & Fukahata, 2011), while others break a network of faults and/or have heterogeneous slip distribution (Li et al., 1994; Ammon et al., 2005; Meng et al., 2012; Cesca et al., 2017). Although the complexity of earthquakes can be directly observed, in some cases, from surface fault trace (Massonnet et al., 1993; Li et al., 1994; Kaneko et al., 2017), many ruptures are buried at depth so that seismic waves are the only observations available to infer the source process. Derived from seismic waves through waveform deconvolution or kinematic inversion, the earthquake Source Time Function (STF) is a foremost important seismic observation that describes the time history of moment release during a rupture. Moreover, the shape of the STF directly controls the variability and uncertainty in the strength and duration of strong ground motion.

Observations of global earthquake STFs and source spectra have shown significant inter-event variability among earthquakes (Allmann & Shearer, 2009; Atik et al., 2010; Denolle, 2019). Such variability may partly come from differences in data processing strategy (Ide & Beroza, 2001). Therefore, large catalogs of STFs (or their spectra) obtained from a uniform approach is preferable to analyze relative differences among earthquakes (Allmann & Shearer, 2009; Convers & Newman, 2011; Denolle & Shearer, 2016; Vallée & Douet, 2016).

62 Recently, such catalogs of STF<sub>s</sub> (or of their spectra) have enabled multiple discov-  
 63 eries about earthquake source processes. For example, the total seismic moment  $M_0$  (the  
 64 time integral of the STF) scales with source duration  $T^3$  (the duration of the STF) for  
 65 most small to moderate size earthquakes, which implies that the earthquake stress drop  
 66 is roughly invariant with earthquake magnitudes. At larger magnitudes, this scaling may  
 67 differ (e.g.  $M_0 \sim T^2$  from Denolle and Shearer (2016)). Their properties also have in-  
 68 dicated that the ratio of the radiated energy  $E_R$  over the moment, also referred to as the  
 69 scaled energy  $E_R/M_0$ , varies spatially and with depth but remains invariant with earth-  
 70 quake magnitude (Convers & Newman, 2011; Baltay et al., 2014; Denolle & Shearer, 2016).

71 However, both the amplitude and the source duration of the STF vary by orders  
 72 of magnitude. This requires careful strategies of amplitude and time scaling for across-  
 73 magnitude visualization and comparison. One approach is to scale the time axis to a du-  
 74 ration metric and normalize the amplitude to seismic moment (i.e. the integral of the  
 75 STF). However, source duration is difficult to measure because near-source and near-site  
 76 scattering of seismic waves may interfere with waves radiating from the end of the seis-  
 77 mic rupture. Therefore previous studies have proposed several metrics of duration: moment-  
 78 based duration (Houston, 2001), threshold-based duration (Vallée, 2013; Denolle, 2019),  
 79 and centroid-based duration (Meier et al., 2017). Because these measures are not strictly  
 80 equivalent, the shapes of the scaled and stretched STF<sub>s</sub> differ as well. For instance, Meier  
 81 et al. (2017) find that average STF<sub>s</sub> have rather a triangle shape whereas Denolle (2019)  
 82 suggests a rather skewed-Gaussian functional form.

83 Here, we propose to weaken the assumption of a particular definition of source du-  
 84 ration and instead use dynamic time warping (DTW) to compare the shapes of the STF<sub>s</sub>.  
 85 DTW has been widely used in speech recognition (Berndt & Clifford, 1994; “Dynamic  
 86 Time Warping”, 2007). The DTW algorithm performs a non-uniform stretching of time  
 87 and amplitude to match the shape of two time series via the optimal warping path with  
 88 minimum distance (Figure S1). We measure the similarity between STF<sub>s</sub> with DTW dis-  
 89 tance and cluster the STF<sub>s</sub> accordingly. We apply this to the global SCARDEC cata-  
 90 log of STF<sub>s</sub> (Vallée & Douet, 2016, available at [http://scardec.projects.sismo.ipgg](http://scardec.projects.sismo.ipgg.fr/)  
 91 [.fr/](http://scardec.projects.sismo.ipgg.fr/), last accessed 01/20/2020) that contains 3529 earthquakes of magnitude greater  
 92 than 5.5 from 1/1/1992 and until 12/31/2018. The analysis shows that the STF over-  
 93 all shape is correlated with several earthquake source parameters, such as focal mech-  
 94 anisms, depth, and scaled energy.

95 To test whether the current physical understanding of earthquake processes repro-  
 96 duces the clustering patterns, we perform dynamic simulations of earthquake ruptures  
 97 with linear slip-weakening friction to construct synthetic STF<sub>s</sub>. We find a strong cor-  
 98 relation between the grouping distribution of STF shapes and frictional parameters, such  
 99 as the characteristic slip-weakening distance  $D_c$ . Furthermore, we find that the group-  
 100 ing pattern of the SCARDEC STF shapes are most similar to those simulated STF<sub>s</sub> with  
 101 small values of  $D_c$ , thus the grouping patterns of a large number of STF<sub>s</sub> can potentially  
 102 provide observational constraints to earthquake dynamics.

## 103 2 Dynamic time warping and clustering analysis

104 DTW measures the similarity between two time series that may not share the same  
 105 frequency content or the same sampling rate. The series are “warped” (or stretched) non-  
 106 uniformly in the time dimensions to optimally match two series (Figure S1). This algo-  
 107 rithm is widely used in automated speech recognition in which different audio sequences  
 108 may have different speaking speeds (Berndt & Clifford, 1994; “Dynamic Time Warping”,  
 109 2007). One important advantage of DTW is its ability to preserve topological structures  
 110 of the time series by assimilating their temporal elongation or compression. Once stretched,  
 111 the DTW distance is taken as a new metric for STF similarity, which can be used for

112 clustering. Our approach follows four steps: 1) STF pre-conditioning, 2) DTW distance  
113 calculation, 3) clustering, 4) re-grouping around a centroid event.

114 We first perform minimal pre-conditioning of the STF shapes. The STFs are built  
115 from the deconvolution of teleseismic P waves that are relatively well constrained at fre-  
116 quencies below 1 Hz (Vallée & Douet, 2016). Given that the maximum duration of the  
117 STF in the catalog is about 100 s, we re-sample the data to 100 points giving a mini-  
118 mum sampling rate of 1 point per second. We then normalize the amplitude STFs to the  
119 event seismic moment. These two processing steps improve the stability of the warping.  
120 We have tested various strategies to resample and normalize the STFs, which did not  
121 affect the conclusions of this analysis.

122 Second, we apply the DTW to each pair of STFs. The DTW distance is the Eu-  
123 clidean distance between two STFs warped along the optimal warping path, and is cho-  
124 sen here as the measure of similarity between two STFs (see Figure S1 (a)-(b)).

125 Then, the STF shapes are clustered based on their DTW distance with a single-  
126 linkage hierarchical clustering analysis that provides the flexibility to form clusters at  
127 any desired level (Text S1, Figure S1 (c)). Here, we constrain the number of clusters to  
128 be 20, which is about equivalent of DTW distance threshold of 0.4. For each of these clus-  
129 ters, we choose a representative STF (defined as the centroid event) that has the min-  
130 imum median distance with all of the other members of the cluster. It is similar to the  
131 stack of all stretched STF within each cluster (Figure 1), which, in turn, exhibits the com-  
132 mon features of all cluster members.

133 Furthermore, we parameterize the characteristic STF shape for each of these clus-  
134 ters by calculating the number of prominent peaks of each centroid event. The number  
135 of prominent peaks is commonly used for topographic relief analysis and is defined as  
136 the amplitude of the peak (hill summit) relative to the lowest amplitude point (valley)  
137 that does not contain a higher peak. This metric differs from the calculation of Gaus-  
138 sian subevents that Danré et al. (2019) use. One hyper-parameter we tune is a thresh-  
139 old for peak amplitude of the prominent peak, which we choose to be 10% of the global  
140 maximum of the STF amplitude. The raw and stretched STFs have a lot fewer promi-  
141 nent peaks than individual peaks from the Gaussian decomposition by Danré et al. (2019)  
142 (Figure S2). Furthermore, the stretched STFs have fewer prominent peaks than the raw  
143 STFs, but in general the same number of prominent peaks as the centroid event (Fig-  
144 ure S3). For instance, a STF may have multiple separated amplitude peaks, but only one  
145 single prominent peak (Figure 1 (a)-(b)).

146 Finally, we group the clusters based on the number of prominent peaks of the cen-  
147 troid event, where G1 is the group where the centroid event has 1 prominent peak, G2  
148 is the group where the centroid event has 2 prominent peaks, ... (Figure 1 (c)). G4 is  
149 the group where the centroid event has at least 4 prominent peaks. Examples of detected  
150 prominent peaks are found in Figure 1 (a)-(b) (see Figure S4 for the unstretched STFs).  
151 In this study, we define the STFs to be “complex” if their DTW stretched STFs have  
152 multiple prominent peak. The first order result from the grouping is that most events  
153 have a single prominent peak whereas about 20% events are more complex.

### 154 **3 Correlations between shape complexity and source parameters**

155 We now explore the correlation between grouping and several source parameters  
156 such as depth, focal mechanism, moment, duration, energy, and location.

157 The first property we investigate is the source depth. Complex STFs (groups G2-  
158 G4) are mostly shallow crustal events ( $\leq 20$  km) whereas the simple STFs (group G1)  
159 can be found at all depths (Figure 2 (a)). Because co-located events have various degrees

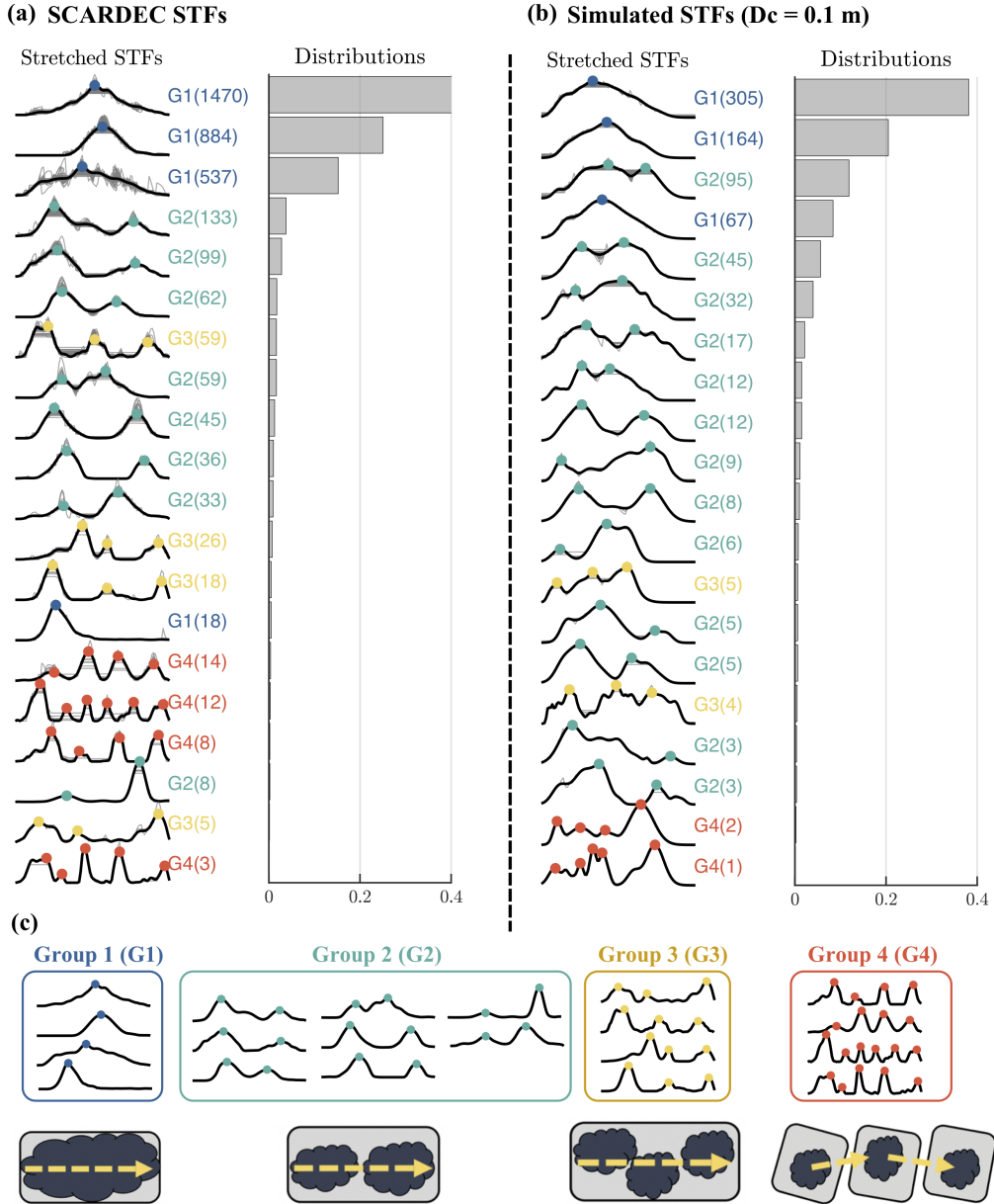


**Figure 1.** Source time function clustering, grouping, and conceptual interpretation. (a) Individual STFs after dynamic time warping and clustering are shown by gray thin lines. Black thick lines are the STFs of the centroid event of each cluster. Colored dots indicate the prominent peaks of the centroid STF as well as the associated group. Numbers in the parentheses are the number of STFs in each cluster. The corresponding population proportion of each cluster is shown in the right histograms. (b) Same as (a) but for the STFs from our dynamic simulations. (c) Cluster centroid STF shapes and conceptual models for G1-G4. In the model diagram, dark blocks represent major rupture asperities and the arrow indicates the rupture direction.

160 of complexity (Figure 2 (d), Figure 3), inaccuracy in the Green's function does not strongly  
 161 bias these specific results.

162 The second property we investigate is the focal mechanism (Figure 2 (b)). The fo-  
 163 cal mechanisms are solved simultaneously by the SCARDEC method (Vallée et al., 2011).  
 164 Most of the thrust earthquakes have simple STF's (G1 and G2), whereas the strike-slip  
 165 earthquakes are dominated by complex STF's (G3 and G4). There are too few normal  
 166 events in the database (only 17.5 %) to give any significant conclusion regarding this  
 167 mechanism.

168 There is no clear relation between earthquake size (moment) and this metric of com-  
 169 plexity (see Figure 2 (d) and Figure S5). For example in Figure 2 (d), we see that the  
 170 largest events in SCARDEC database may only have one prominent peak in their stretched  
 171 STF, while the events with smaller moments can be in any of those complexity groups.

172 We find a clear pattern that G3-G4 events have an abnormally longer duration with  
 173 respect to other events of similar magnitudes and relative to events of the other groups  
 174 (Figure 2 (d)). It is illustrated in Figure 2 (d) by visualization of two STF's of co-located  
 175 events and of similar magnitudes. For the same earthquake moment (or the STF inte-  
 176 gral), it is intuitive to understand that STF's in G4 have multiple low amplitude promi-  
 177 nent peaks and overall extended duration, compared to the G1 STF's that have a sin-  
 178 gle high amplitude and short duration peak. Simple models of crack ruptures yield a re-  
 179 lation between moment, source duration, and stress drop that could indicate low stress  
 180 drops for the G4 events (Figure S6 (a)-(c)) (Brune, 1971; Eshelby, 1957).

181 We now explore the clustering results against the earthquake scaled energy. Here  
 182 we calculate radiated energy from the squared time derivative of the STF (moment ac-  
 183 celeration function  $\ddot{M}_0(t)$ ) using the relation  $E_R = (\frac{1}{15\pi\rho V_p^5} + \frac{1}{10\pi\rho V_s^5}) \int_0^\infty (\ddot{M}_0(t))^2 dt$ .  
 184 We select depth-dependent bulk properties ( $V_p$ ,  $V_s$ ,  $\rho$ ) from PREM (Dziewonski & An-  
 185 derson, 1981). Radiated energy scales almost linearly with seismic moment and look at  
 186 the scaled energy, the ratio of both radiated energy and seismic moment. Figure 2 (c)  
 187 shows the distribution of the scaled energy with respect to each group. G3 and G4 events  
 188 have systematically larger scaled energy as G1 and G2 events. This is consistent with  
 189 intuition that G3 and G4 events generally have rougher STF's.

190 The correlations between STF complexity and source depths and focal mechanism  
 191 are consistent with the findings from previous studies (Houston, 2001; Vallée, 2013; Danré  
 192 et al., 2019). In particular, shallow strike slip earthquakes are constrained geometrically  
 193 by the Earth surface on the top and the seismogenic depth on the bottom. They also  
 194 tend to be composed of segmented faults (Klinger, 2010). These geometrical settings con-  
 195 trol the evolution of rupture that tends to operate with moving energetic slip pulses (Kaneko  
 196 & Lapusta, 2010) with repeated rupture acceleration and deceleration as they travel across  
 197 segments (e.g., Kanamori et al., 1992; Peyrat et al., 2001; Cesca et al., 2017).

198 Since earthquake source parameters are closely related to the local tectonic regime,  
 199 we also find that our observations from the clustering and grouping results (G1 - G4)  
 200 are consistent to the marked variation of tectonic environments (Figure 3). Many of the  
 201 major subduction zones are dominated by the simpler types of events (G1 and G2) and  
 202 lack of more complex ones, likely because they are dominated by thrust events located  
 203 along/within the subducting slabs at various depths. For example, since 1992, there have  
 204 been only two events ( $M_W > 5.5$ ) belonging to the G3 group along the Southern Amer-  
 205 ican and Aleutian subduction zones, respectively (Figure 4 (a)-(b)). Similarly, other sub-  
 206 duction zone regions like in Japan and in Sumatra, the Indian-Eurasian collision zone  
 207 are also dominated by simple-type earthquakes (Figure 4 (c)-(d)). In contrast, the com-  
 208 plex group (G3 and G4) events are located mostly along the boundaries around the junc-  
 209 tion region of the Indo-Australian, western Pacific, Philippine plates and Eurasian plates  
 210 (Figure 3 and Figure 4 (e)). Bird (2003) explored and documented the kinematics at plate  
 211 boundaries and found that this region is characterized by a particularly extensive num-  
 212 ber of micro plates, whose boundaries exhibit varied relative motions and kinematics (their

213 Figure 6). Therefore, we propose that the complexity in the STF may reflect the com-  
 214 plexity in the regional stress field.

#### 215 4 Modeling STF complexity

216 Simulations of dynamic ruptures using stochastic distributions of fault-interface pa-  
 217 rameters are popular in the investigations of complex kinematic source models, realis-  
 218 tic fault geometry and roughness models, and to simulate high-frequency ground motions  
 219 (Mai & Beroza, 2002; Ripperger et al., 2007; Trugman & Dunham, 2014; Graves & Pitarka,  
 220 2016; Mai et al., 2017). In order to investigate possible factors that control the STF com-  
 221 plexity patterns, we perform a large number of 2-dimensional dynamic rupture simula-  
 222 tions with stochastic distributions of pre-stress, and apply the same clustering analysis  
 223 to the resulting synthetic STFs as to the SCARDEC STFs.

224 In this study, synthetic dynamic sources are generated in a 2-dimensional medium  
 225 in an anti-plane setting. Pre-stress on the fault is constrained to follow a power-law am-  
 226 plitude distribution that approximates the scenario caused by natural fault roughness  
 227 (Candela et al., 2012, Text S2 for more details). We assume a constant normal stress of  
 228 120 MPa and linear slip weakening friction law (Andrews, 1976). Linear slip weakening  
 229 requires three parameters: the static friction coefficient (here chosen as  $\mu_s = 0.677$ ),  
 230 the dynamic friction coefficient (here chosen as  $\mu_d = 0.525$ ), and the characteristic slip-  
 231 weakening distance  $D_c$ . We set up the experiments so that the fault-average stress drop  
 232 is about 1 MPa (Figure S7).

233 Danré et al. (2019) find that heterogeneity is necessary to reproduce realistically  
 234 rough STFs. Here, we focus on varying  $D_c$ , yet aware of the trade-off between strength  
 235 excess and  $D_c$  in controlling rupture velocity and the resulting ground motions (Guatterri  
 236 & Spudich, 2000). While we keep  $D_c$  constant within a single set of simulations, we carry  
 237 several sets of experiments with values of  $D_c$  at various levels 0.05, 0.1, 0.2, 0.4, 0.8, and  
 238 1.6 m that are within bounds found in the literature.

239 For each  $D_c$ , we first generate a set of pre-stress distributions that we use in each  
 240 simulations. The dynamic rupture is solved by 2D boundary integral method SBIEM-  
 241 LAB (<http://web.gps.caltech.edu/~ampuero/software.html>, last accessed 11/27/2018).  
 242 We discard the rupture models that unsuccessfully nucleated with a source dimension  
 243 less than 20 km, or rupture beyond the zone of heterogeneous pre-stress, and obtain 800  
 244 qualified simulations for each  $D_c$  value. Finally, the STFs are calculated from the inte-  
 245 gral of the moment-density-rate functions over the fault surface (more details in Text  
 246 S2).

247 We perform the hierarchical clustering and group the simulated STFs for each  $D_c$ ,  
 248 following the same procedures as for the SCARDEC STFs (Figure 1 (b), Figures S8 -  
 249 S12). Because our modeling is not three dimensional and does not include the free sur-  
 250 face, we are not matching observations such as the focal mechanism and depth. How-  
 251 ever, our results can match the proportion of the STFs relative to each group: 80% of  
 252 the STFs belong to the G1 group, 15% belong to the G2, and the rest in higher indexed  
 253 groups. Comparison of the relative proportion between groups for each set of simulations  
 254 suggests that an increasing  $D_c$  value yield an increase in STF complexity (e.g. propor-  
 255 tion of G3-G4 events). This shows that  $D_c$ , or more generally, the frictional parameters  
 256 can impact the complexity of STFs. Compared with the observed global variability in  
 257 SCARDEC STFs, small value of  $D_c$  ( $< 0.1$  m) is preferred in this particular metric of  
 258 complexity. In contrast, models with large value of  $D_c$  tend to generate proportionally  
 259 more STFs belonging to G3 beyond (Figures S10 - S12).

260 Our results indicate that the small values of  $D_c < 0.1$  m are necessary to produce  
 261 the general level of complexity of the SCARDEC STFs (Figure 5 (a)). When binning  
 262 these relative contributions with source depths, we find that crustal events ( $h \leq 40$  km),

263 which show a higher degree of complexity, could be explained by a larger  $D_c$  value than  
 264 the deeper events (Figure 2 (a), Figure 5 (b)). This is more pronounced with the upper-  
 265 crustal depths ( $h \leq 20$  km).

266 Depth variations in  $D_c$  have been reported in earlier studies. Wibberley and Shi-  
 267 mamoto (2005) perform laboratory experiments on samples from the Median Tectonic  
 268 Line in southwestern Japan, and estimate that  $D_c$  ought to vary with depth, with a deeper  
 269 (6 km) values being systematically 30% smaller than the shallow (2 km) values. Kine-  
 270 matic source inversions also find a systematic depth variation of rise time, which they  
 271 attribute to a systematic dependence in  $D_c$  (Ide & Takeo, 1997). Our results may pro-  
 272 vide a supporting evidence that the characteristic slip-weakening distance varies at depth  
 273 over crustal scales.

## 274 5 Discussion and Conclusion

275 We apply a dynamic time warping methodology to cluster a large number of earth-  
 276 quake source time functions based on similarity of their general shapes. We find patterns  
 277 between source parameters and the STF shape, which we now compare with previous  
 278 work Danré et al. (2019) that analyzed the same SCARDEC database. Although the def-  
 279 inition of complexity in Danré et al. (2019) is different, this study confirms the corre-  
 280 lation between STF complexity with focal depth and mechanisms. This study adds to  
 281 the Danré et al. (2019) in three ways. First, there is no correlation between this partic-  
 282 ular metric of complexity and earthquake magnitude. This means that the shape of the  
 283 individual prominent peaks does not systematically change with earthquake magnitude,  
 284 while the number of individual and separated peaks does. Second, we analyze in this study  
 285 the relation between degree of complexity and other source parameters, such as the scal-  
 286 ing between duration and moment (sometimes used to estimate earthquake stress drop)  
 287 and the ratio between radiated energy and moment. Taken together, it is reasonable to  
 288 infer that the complex STFs exhibit large radiation ratio (proportion of radiated energy  
 289 over available energy).

290 Finally, the modeled STFs exhibit different degrees of complexity depending on the  
 291 frictional properties. We find that small values of characteristic slip weakening distance  
 292 are required to reproduce the variability in complexity measured in the SCARDEC database.  
 293 Furthermore, we find that the variability in STF complexity of shallow earthquakes is  
 294 better explained by a larger value of characteristic distance compared to the deeper sources.

295 There are several limitations to our approaches. First, the database we use is con-  
 296 structed from a Green's function in a radially symmetric Earth. Although this is unlikely  
 297 to affect the overall results, Green's functions that account for laterally varying struc-  
 298 ture would improve the temporal resolution of the shallowest events. This requires bet-  
 299 ter understanding of near surface scattering and attenuation. Second, our modeling ap-  
 300 proach is unable to characterize the correlation between focal mechanisms and STF com-  
 301 plexity. Indeed, these parameters could be tested using a 3-dimensional dynamic rup-  
 302 ture simulation framework, which however is impractical to implement due to high com-  
 303 putational expense and the employed statistical approaches. Nevertheless, because fault  
 304 geometry and fault properties seem to play a dominant role in shaping the source and  
 305 the resulting strong ground motions, further 3-dimensional modeling and observations  
 306 are necessary.

## 307 Acknowledgments

308 We sincerely thank Martin Vallée for his insightful suggestions. All the source time func-  
 309 tions are downloaded from SCARDEC source time function database (<http://scardec.projects.sismo.ipgp.fr/>). The dynamic rupture simulation code SBIEMLAB is de-  
 310 veloped by Jean-Paul Ampuero (available on <http://web.gps.caltech.edu/~ampuero/>)  
 311

312 software.html). The Matlab scripts to reproduce the results and figures can be obtained  
 313 on the Github ([https://github.com/yinjiuxun/STF\\_DTW](https://github.com/yinjiuxun/STF_DTW)). Global maps are made by  
 314 GMT (Wessel et al., 2013, available at <http://gmt.soest.hawaii.edu/>).

## 315 References

- 316 Allmann, B. P., & Shearer, P. M. (2009). Global variations of stress drop for mod-  
 317 erate to large earthquakes. *Journal of Geophysical Research: Solid Earth*,  
 318 *114*(B1), B01310. doi: 10.1029/2008JB005821
- 319 Ammon, C. J., Ji, C., Thio, H.-K., Robinson, D., Ni, S., Hjorleifsdottir, V., ...  
 320 Wald, D. (2005). Rupture Process of the 2004 Sumatra-Andaman Earthquake.  
 321 *Science*, *308*(5725), 1133–1139. doi: 10.1126/science.1112260
- 322 Andrews, D. J. (1976). Rupture propagation with finite stress in antiplane  
 323 strain. *Journal of Geophysical Research*, *81*(20), 3575–3582. doi: 10.1029/  
 324 JB081i020p03575
- 325 Atik, L. A., Abrahamson, N., Bommer, J. J., Scherbaum, F., Cotton, F., & Kuehn,  
 326 N. (2010). The Variability of Ground-Motion Prediction Models and  
 327 Its Components. *Seismological Research Letters*, *81*(5), 794–801. doi:  
 328 10.1785/gssrl.81.5.794
- 329 Baltay, A. S., Beroza, G. C., & Ide, S. (2014). Radiated Energy of Great Earth-  
 330 quakes from Teleseismic Empirical Green’s Function Deconvolution. *Pure and*  
 331 *Applied Geophysics*, *171*(10), 2841–2862. doi: 10.1007/s00024-014-0804-0
- 332 Berndt, D. J., & Clifford, J. (1994). Using dynamic time warping to find patterns in  
 333 time series. In *KDD workshop* (Vol. 10, pp. 359–370). Seattle, WA.
- 334 Bird, P. (2003). An updated digital model of plate boundaries. *Geochemistry, Geo-*  
 335 *physics, Geosystems*, *4*(3). doi: 10.1029/2001GC000252
- 336 Brune, J. N. (1971). Correction (to Brune, 1970). *J. geophys. Res.*, *76*, 5002.
- 337 Candela, T., Renard, F., Klinger, Y., Mair, K., Schmittbuhl, J., & Brodsky, E. E.  
 338 (2012). Roughness of fault surfaces over nine decades of length scales. *Journal*  
 339 *of Geophysical Research: Solid Earth*, *117*(B8). doi: 10.1029/2011JB009041
- 340 Cesca, S., Zhang, Y., Mouslopoulou, V., Wang, R., Saul, J., Savage, M., ... Dahm,  
 341 T. (2017). Complex rupture process of the Mw 7.8, 2016, Kaikoura earth-  
 342 quake, New Zealand, and its aftershock sequence. *Earth and Planetary Science*  
 343 *Letters*, *478*, 110–120. doi: 10.1016/j.epsl.2017.08.024
- 344 Convers, J. A., & Newman, A. V. (2011). Global evaluation of large earthquake en-  
 345 ergy from 1997 through mid-2010. *J. Geophys. Res. Solid Earth*. doi: 10.1029/  
 346 2010JB007928
- 347 Danré, P., Yin, J., Lipovsky, B. P., & Denolle, M. A. (2019). Earthquakes Within  
 348 Earthquakes: Patterns in Rupture Complexity. *Geophysical Research Letters*,  
 349 *46*(13), 7352–7360. doi: 10.1029/2019GL083093
- 350 Denolle, M. A. (2019). Energetic Onset of Earthquakes. *Geophysical Research Let-*  
 351 *ters*, *46*(5), 2458–2466. doi: 10.1029/2018GL080687
- 352 Denolle, M. A., & Shearer, P. M. (2016). New perspectives on self-similarity for  
 353 shallow thrust earthquakes. *Journal of Geophysical Research: Solid Earth*,  
 354 *121*(9), 2016JB013105. doi: 10.1002/2016JB013105
- 355 Dynamic Time Warping. (2007). In M. Müller (Ed.), *Information Retrieval for Mu-*  
 356 *sic and Motion* (pp. 69–84). Berlin, Heidelberg: Springer. doi: 10.1007/978-3-  
 357 -540-74048-3\_4
- 358 Dziewonski, A. M., & Anderson, D. L. (1981). Preliminary reference Earth  
 359 model. *Physics of the Earth and Planetary Interiors*, *25*(4), 297–356. doi:  
 360 10.1016/0031-9201(81)90046-7
- 361 Eshelby, J. D. (1957). The determination of the elastic field of an ellipsoidal inclu-  
 362 sion, and related problems. In *Proceedings of the Royal Society of London A:*  
 363 *Mathematical, Physical and Engineering Sciences* (Vol. 241, pp. 376–396). The  
 364 Royal Society.

- 365 Graves, R., & Pitarka, A. (2016). Kinematic Ground-Motion Simulations on Rough  
366 Faults Including Effects of 3d Stochastic Velocity Perturbations Kinematic  
367 Ground-Motion Simulations on Rough Faults. *Bulletin of the Seismological*  
368 *Society of America*, *106*(5), 2136–2153. doi: 10.1785/0120160088
- 369 Guatteri, M., & Spudich, P. (2000). What Can Strong-Motion Data Tell Us about  
370 Slip-Weakening Fault-Friction Laws? *Bulletin of the Seismological Society of*  
371 *America*, *90*(1), 98–116. doi: 10.1785/0119990053
- 372 Houston, H. (2001). Influence of depth, focal mechanism, and tectonic setting  
373 on the shape and duration of earthquake source time functions. *Journal of*  
374 *Geophysical Research: Solid Earth*, *106*(B6), 11137–11150. doi:  
375 10.1029/2000JB900468
- 376 Ide, S., & Beroza, G. C. (2001). Does apparent stress vary with earthquake size.  
377 *Geophys. Res. Lett.*, *28*(17), 3349–3352.
- 378 Ide, S., & Takeo, M. (1997). Determination of constitutive relations of fault slip  
379 based on seismic wave analysis. *Journal of Geophysical Research: Solid Earth*,  
380 *102*(B12), 27379–27391. doi: 10.1029/97JB02675
- 381 Kanamori, H., Hong-Kie, T., Doug, D., Egill, H., & Heaton, T. (1992). Initial  
382 investigation of the Landers, California, Earthquake of 28 June 1992 us-  
383 ing TERRAscope. *Geophysical Research Letters*, *19*(22), 2267–2270. doi:  
384 10.1029/92GL02320
- 385 Kaneko, Y., Fukuyama, E., & Hamling, I. J. (2017). Slip-weakening distance and  
386 energy budget inferred from near-fault ground deformation during the 2016  
387 Mw7.8 Kaikōura earthquake. *Geophysical Research Letters*, *44*(10), 4765–4773.  
388 doi: 10.1002/2017GL073681
- 389 Kaneko, Y., & Lapusta, N. (2010). Supershear transition due to a free surface in  
390 3-D simulations of spontaneous dynamic rupture on vertical strike-slip faults.  
391 *Tectonophysics*, *493*(3), 272–284. doi: 10.1016/j.tecto.2010.06.015
- 392 Klinger, Y. (2010). Relation between continental strike-slip earthquake segmenta-  
393 tion and thickness of the crust. *Journal of Geophysical Research: Solid Earth*,  
394 *115*(B7). doi: 10.1029/2009JB006550
- 395 Li, Y.-G., Aki, K., Vidale, J. E., Lee, W. H. K., & Marone, C. J. (1994). Fine Struc-  
396 ture of the Landers Fault Zone: Segmentation and the Rupture Process. *Sci-*  
397 *ence*, *265*(5170), 367–370. doi: 10.1126/science.265.5170.367
- 398 Mai, P. M., & Beroza, G. C. (2002). A spatial random field model to characterize  
399 complexity in earthquake slip. *Journal of Geophysical Research: Solid Earth*,  
400 *107*(B11), ESE 10–1. doi: 10.1029/2001JB000588
- 401 Mai, P. M., Galis, M., Thingbaijam, K. K. S., Vyas, J. C., & Dunham, E. M.  
402 (2017). Accounting for Fault Roughness in Pseudo-Dynamic Ground-  
403 Motion Simulations. *Pure and Applied Geophysics*, *174*(9), 3419–3450. doi:  
404 10.1007/s00024-017-1536-8
- 405 Massonnet, D., Rossi, M., Carmona, C., Adragna, F., Peltzer, G., Feigl, K., &  
406 Rabaute, T. (1993). The displacement field of the Landers earthquake mapped  
407 by radar interferometry. *Nature*, *364*(6433), 138–142. doi: 10.1038/364138a0
- 408 Meier, M.-A., Ampuero, J. P., & Heaton, T. H. (2017). The hidden simplicity of  
409 subduction megathrust earthquakes. *Science*, *357*(6357), 1277–1281. doi: 10  
410 .1126/science.aan5643
- 411 Meng, L., Ampuero, J.-P., Stock, J., Duputel, Z., Luo, Y., & Tsai, V. C. (2012).  
412 Earthquake in a maze: Compressional rupture branching during the 2012 Mw  
413 8.6 Sumatra earthquake. *Science*, *337*(6095), 724–726.
- 414 Peyrat, S., Olsen, K., & Madariaga, R. (2001, November). Dynamic modeling of  
415 the 1992 Landers earthquake. *Journal of Geophysical Research: Solid Earth*,  
416 *106*(B11), 26467–26482. doi: 10.1029/2001JB000205
- 417 Ripperger, J., Ampuero, J.-P., Mai, P. M., & Giardini, D. (2007). Earthquake  
418 source characteristics from dynamic rupture with constrained stochastic  
419 fault stress. *Journal of Geophysical Research: Solid Earth*, *112*(B4). doi:

- 420 10.1029/2006JB004515  
421 Shearer, P. M., Prieto, G. A., & Hauksson, E. (2006). Comprehensive analysis of  
422 earthquake source spectra in southern California. *Journal of Geophysical Re-*  
423 *search: Solid Earth*, *111*(B6). doi: 10.1029/2005JB003979
- 424 Trugman, D. T., & Dunham, E. M. (2014). A 2d Pseudodynamic Rupture Model  
425 Generator for Earthquakes on Geometrically Complex Faults A 2d Pseudody-  
426 namic Rupture Model Generator for Earthquakes on Geometrically Complex  
427 Faults. *Bulletin of the Seismological Society of America*, *104*(1), 95–112. doi:  
428 10.1785/0120130138
- 429 Vallée, M. (2013). Source time function properties indicate a strain drop indepen-  
430 dent of earthquake depth and magnitude. *Nature Communications*, *4*, 2606.  
431 doi: 10.1038/ncomms3606
- 432 Vallée, M., Charléty, J., Ferreira, A. M. G., Delouis, B., & Vergoz, J. (2011).  
433 SCARDEC: a new technique for the rapid determination of seismic moment  
434 magnitude, focal mechanism and source time functions for large earthquakes  
435 using body-wave deconvolution. *Geophysical Journal International*, *184*(1),  
436 338–358. doi: 10.1111/j.1365-246X.2010.04836.x
- 437 Vallée, M., & Douet, V. (2016). A new database of source time functions (STFs) ex-  
438 tracted from the SCARDEC method. *Physics of the Earth and Planetary Inte-*  
439 *riors*, *257*, 149–157. doi: 10.1016/j.pepi.2016.05.012
- 440 Wessel, P., Smith, W. H. F., Scharroo, R., Luis, J., & Wobbe, F. (2013). Generic  
441 Mapping Tools: Improved Version Released. *Eos, Transactions American Geo-*  
442 *physical Union*, *94*(45), 409–410. doi: 10.1002/2013EO450001
- 443 Wibberley, C. A. J., & Shimamoto, T. (2005). Earthquake slip weakening and asper-  
444 ities explained by thermal pressurization. *Nature*, *436*(7051), 689–692. doi: 10  
445 .1038/nature03901
- 446 Yagi, Y., & Fukahata, Y. (2011). Rupture process of the 2011 Tohoku-oki earth-  
447 quake and absolute elastic strain release. *Geophysical Research Letters*, *38*(19).  
448 doi: 10.1029/2011GL048701

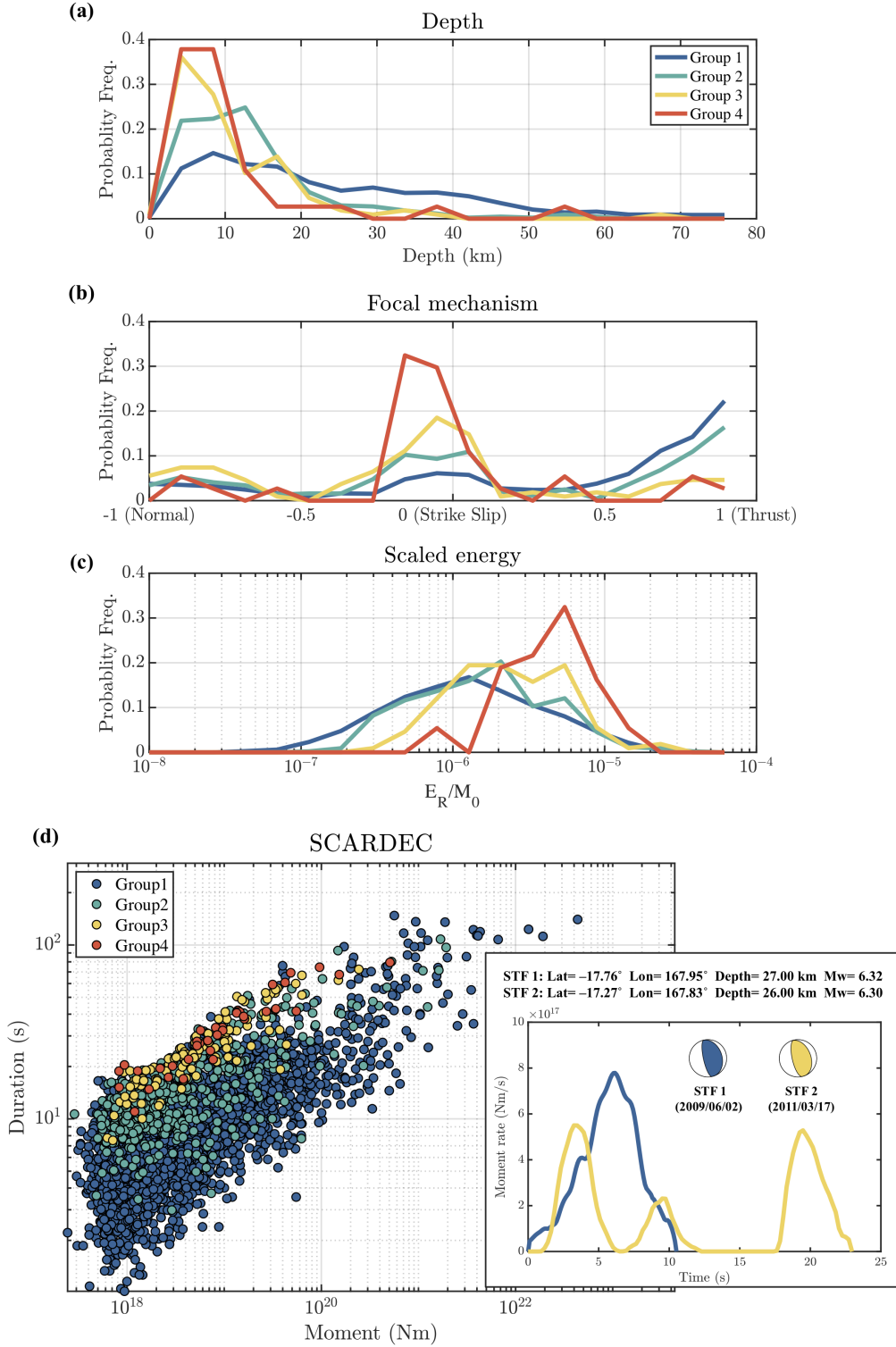


**Figure 2.** Population distribution of four complexity groups and correlation with different source parameters: (a) centroid depth, (b) focal mechanism (scalar defined by Shearer et al. (2006) that varies from -1 (normal), 0 (strike-slip) to 1 (reverse)), (c) and scaled radiated energy  $e = E_R/M_0$ . Panel (d) shows the earthquake duration against earthquake moment, colored with the respective group labels. One pair of co-located events with different complexity are also shown in the inset.

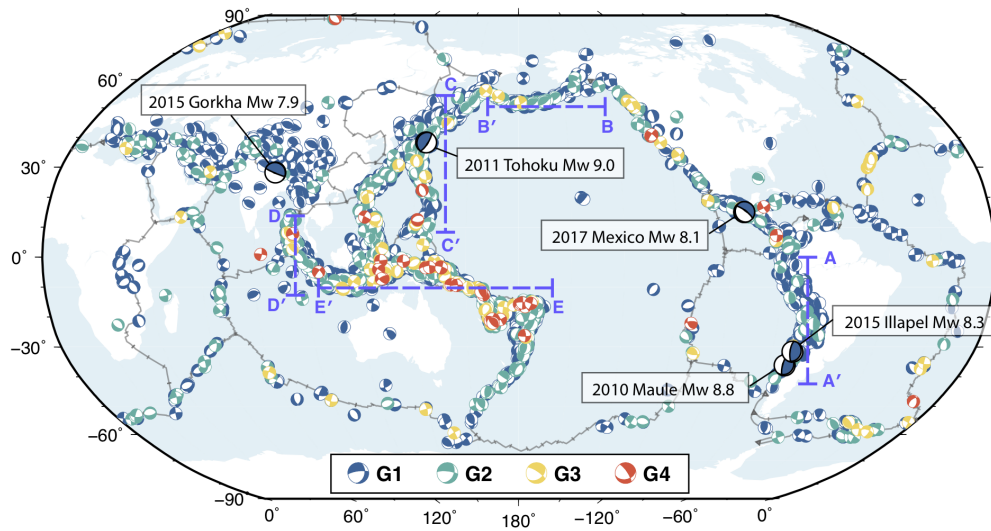


**Figure 3.** Map of focal mechanisms colored by their group label and overlay of the plate boundaries (gray thin lines). Several recent large megathrust earthquakes are highlighted. Blue dashed lines shown the locations of profiles in Figure 4. Bottom panels show the center STFs in each groups (same as those in Figure 1 (a)) as well as the corresponding schematic rupture propagation.

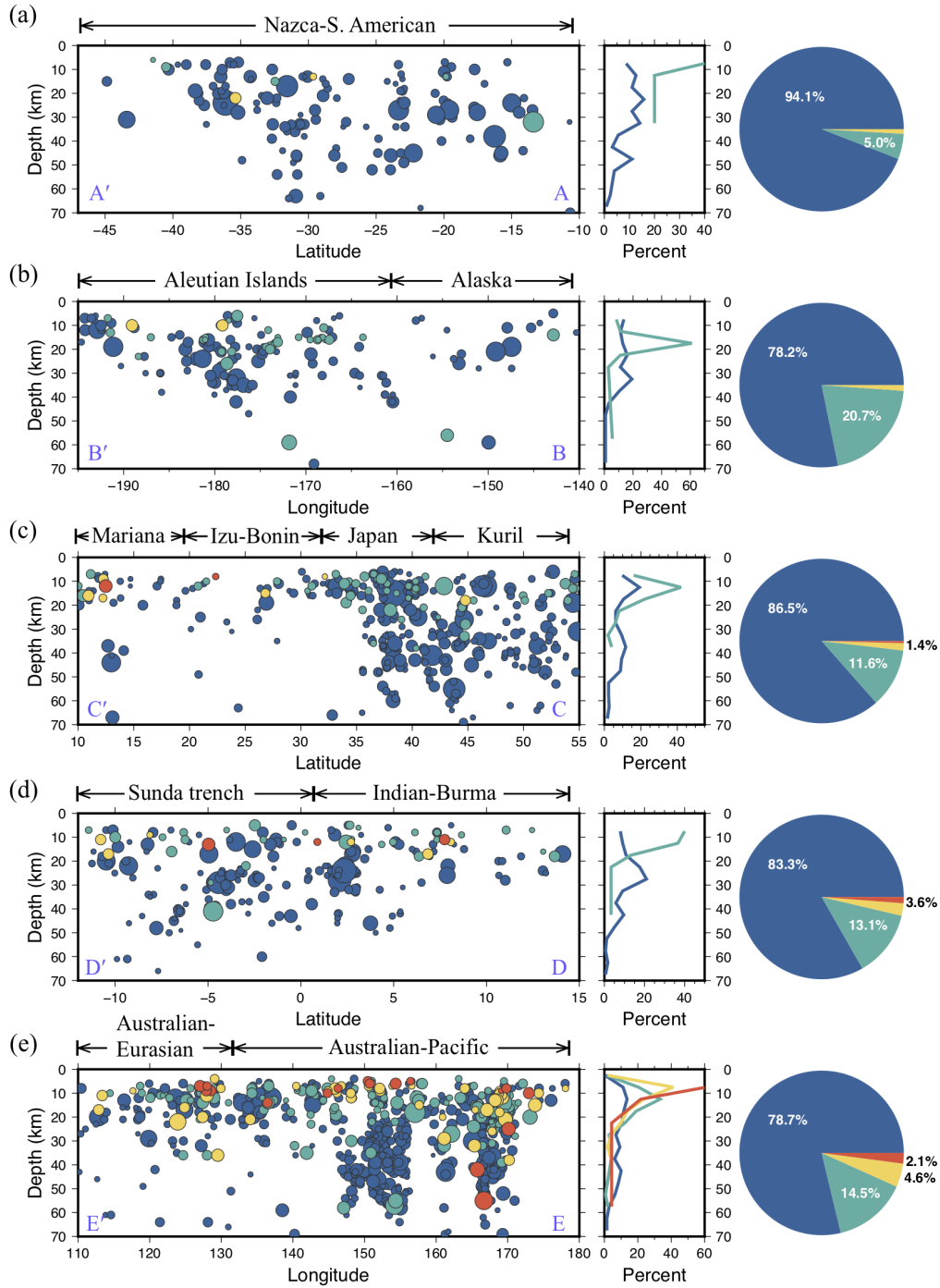


**Figure 4.** Earthquake distributions of different complexity groups on the vertical profiles (from 0–70 km, locations are indicated by blue dashed lines in Figure 3). The regional along-depth and total group distributions are also shown to the right.

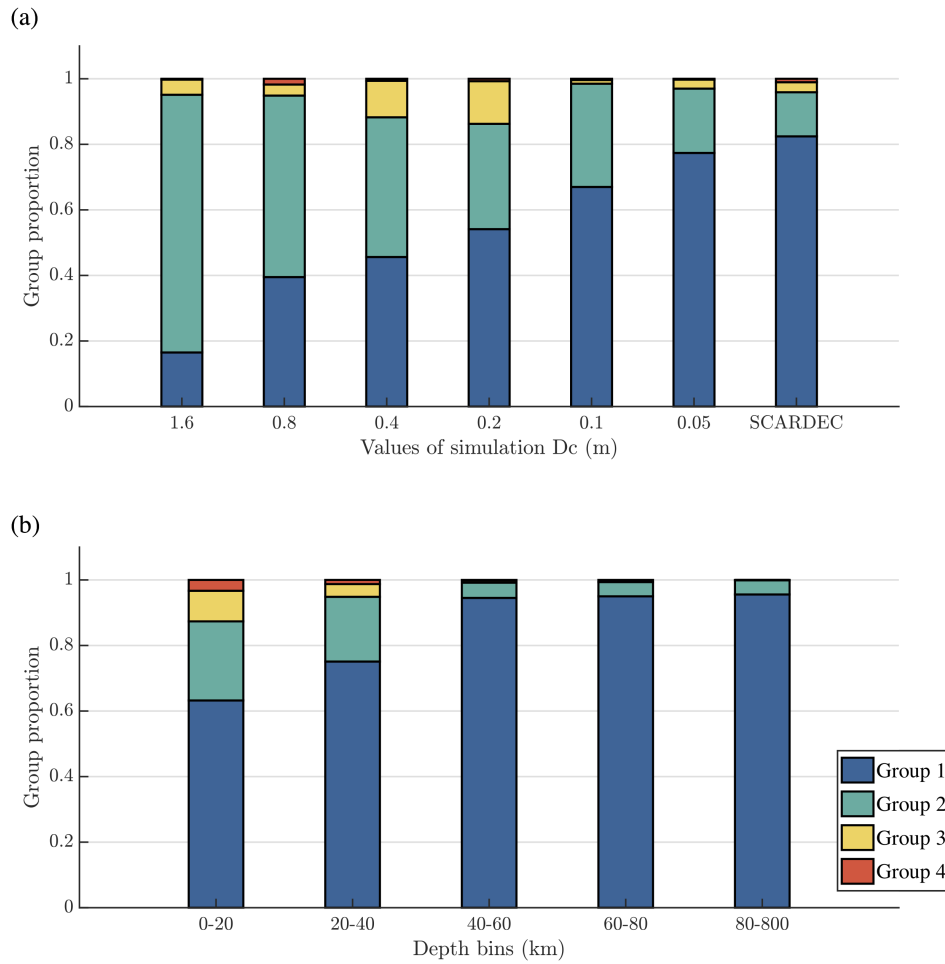


**Figure 5.** Group proportion distributions: (a) simulated STFs clustering with different values of  $D_c$ , compared with the group proportions of real STFs (SCARDEC); (b) Group proportions of real STFs (SCARDEC) within different depth bins.